

Article

Clay Mineralogy of Coal-Hosted Nb-Zr-REE-Ga Mineralized Beds from Late Permian Strata, Eastern Yunnan, SW China: Implications for Paleotemperature and Origin of the Micro-Quartz

Lixin Zhao ^{1,†}, Shifeng Dai ^{1,2,*}, Ian T. Graham ^{3,†} and Peipei Wang ^{1,†}

¹ College of Geoscience and Surveying Engineering, China University of Mining and Technology (Beijing), Beijing 100083, China; TBP120201007@student.cumtb.edu.cn (L.Z.); wangpeipei1100@gmail.com (P.W.)

² State Key Laboratory of Coal Resources and Safe Mining, China University of Mining and Technology (Beijing), Beijing 100083, China

³ School of Biological, Earth and Environmental Sciences, University of New South Wales, Sydney 2052, Australia; i.graham@unsw.edu.au

* Correspondence: daishifeng@gmail.com; Tel.: +86-10-6234-1868

† These authors contributed equally to this work.

Academic Editor: Dimitrina Dimitrova

Received: 24 January 2016; Accepted: 11 May 2016; Published: 17 May 2016

Abstract: The clay mineralogy of pyroclastic Nb(Ta)-Zr(Hf)-REE-Ga mineralization in Late Permian coal-bearing strata from eastern Yunnan Province; southwest China was investigated in this study. Samples from XW and LK drill holes in this area were analyzed using XRD (X-ray diffraction) and SEM (scanning electronic microscope). Results show that clay minerals in the Nb-Zr-REE-Ga mineralized samples are composed of mixed layer illite/smectite (I/S); kaolinite and berthierine. I/S is the major component among the clay assemblages. The source volcanic ashes controlled the modes of occurrence of the clay minerals. Volcanic ash-originated kaolinite and berthierine occur as vermicular and angular particles, respectively. I/S is confined to the matrix and is derived from illitization of smectite which was derived from the original volcanic ashes. Other types of clay minerals including I/S and berthierine precipitated from hydrothermal solutions were found within plant cells; and coexisting with angular berthierine and vermicular kaolinite. Inferred from the fact that most of the I/S is R1 ordered with one case of the R3 I/S; the paleo-diagenetic temperature could be up to 180 °C but mostly 100–160 °C. The micro-crystalline quartz grains (<10 µm) closely associated with I/S were observed under SEM and were most likely the product of desilicization during illitization of smectite.

Keywords: coal-hosted Nb-Zr-REE-Ga mineralization; clay minerals; paleotemperature; microcrystalline quartz

1. Introduction

Polymetallic Nb(Ta)-Zr(Hf)-REE-Ga mineralization within Late Permian coal-bearing strata of eastern Yunnan Province, southwest China was reported by Dai, *et al.* [1]. The Nb(Ta)-Zr(Hf)-REE-Ga mineralization has anomalous response on natural gamma log curves and is widespread at the base of the Wuchiapingian of Late Permian age (*i.e.*, terrestrial Xuanwei and terrestrial-marine transitional Longtan Formations) in southwest China [1–3]. The mineralization is believed to be derived from alkali volcanic ashes and occurs as thick beds (up to 10 m but mostly 2–5 m) interbedded in the sedimentary rocks of terrigenous origin [1]. In most cases, the Nb-Zr-REE-Ga mineralized horizon has been argillized, but tuffaceous textures, volcanic breccia, and hematitization can be observed as

well [1,2]. The Nb-Zr-REE-Ga mineralization occurs within coal-bearing strata and within coal beds directly [3], and accordingly, this Nb(Ta)-Zr(Hf)-REE-Ga polymetallic mineralization was generalized as a coal-hosted rare metal deposit [4].

This Nb-Zr-REE-Ga-enriched mineralization is characterized by significant enrichment in Nb, Ta, Zr, Hf, REE (rare earth elements and Y) and Ga, for example, $(\text{Nb,Ta})_2\text{O}_5$, 0.0302–0.0627 wt %; $(\text{Zr,Hf})\text{O}_2$, 0.3805–0.8468 wt %; REO (oxides of REE), 0.1216–0.1358 wt %; and Ga, 52.4–81.3 ppm [1,3]. Notably, the content of $(\text{Nb,Ta})_2\text{O}_5$ is much higher than the required industrial $(\text{Nb,Ta})_2\text{O}_5$ grade of weathered crust niobium deposits (0.016–0.02 wt %) [5] while the concentration of Ga is also higher than the required Ga industrial grade in coal (30 ppm) and in bauxite (20 ppm) [6]. In most cases, the contents of REO and $(\text{Zr,Hf})_2\text{O}_5$ have also been up to their corresponding industrial utilization grades [5,7].

Although the mineralization of Nb(Ta)-Zr(Hf)-REE-Ga in the study area is notably significant, their hosted minerals such as zircon, pyrochlore, columbite *etc.* are rarely observed within the Nb-Zr-REE-Ga mineralized beds under both the microscope and X-ray diffraction (XRD) [1]. While using scanning electron microscopy (SEM), Dai *et al.* [2] identified several rare metal-bearing minerals including REE-bearing minerals (rhabdophane, silico-rhabdophane, florencite, parasite and xenotime), zircon, and Nb-bearing anatase within the Nb-Zr-REE-Ga mineralization. These rare metal-bearing minerals mainly occur within pores and cavities of clay minerals as very fine dispersed grains (in most cases $<5\ \mu\text{m}$) indicating that they are probably of authigenic origin derived from re-deposition of rare metals leached from the Nb-Zr-REE-Ga-enriched tuff by hydrothermal solutions [2]. However, these rare-metal bearing minerals are rare to be observed under SEM and not in sufficient concentration to explain the high contents of rare metals found in the geochemical analyses, for example, zircon as the only Zr-bearing mineral phase identified by Dai *et al.* [2] was rarely observed in the samples which contain up to thousands of ppm zirconium. On the other hand, the amount of zircon within the Nb(Ta)-Zr(Hf)-REE-Ga-mineralized samples (with Zr in thousands ppm level and Nb in hundreds ppm level) in the lower Xuanwei Formation (the mineralization-bearing strata) is 10–100 times that of the pyroclastic tonsteins which only contain hundreds of ppm Zr and tens of ppm Nb from the upper part of the Xuanwei Formation [8]. Therefore, the majority of rare metals do not occur within discrete mineral phases such as zircon, Nb-anatase, and REE-phosphate/carbonate, and must therefore be inferred to occur as absorbed ions within the clay minerals [1,8,9]. In fact, our unpublished results of leaching experiments showed that the ammonium sulfate solutions could extract a large amount of rare metals from the Nb-Zr-REE-Ga-mineralized samples (though not the specifically studied samples) providing indirect evidence for a certain amount of rare metals being absorbed within clay minerals. Therefore, a detailed study of the clay minerals is required to understand the modes of occurrence and industrial utilization of these rare metal elements. In this paper, we report on the clay mineralogy (species, abundances, modes of occurrence, and ordering of mixed layer illite/smectite) in the Nb-Zr-REE-Ga mineralized beds by an investigation of samples collected from two drill holes (XW and LK) in eastern Yunnan Province, SW China. This paper also provides an insight into the paleo-diagenetic temperature and origin of the ultrafine quartz particles ($<10\ \mu\text{m}$) found in the studied samples.

2. Geological Setting

The ~260 Ma Emeishan Large Igneous Province (ELIP) in SW China is considered to be the result of mantle plume activity and mainly comprises massive flood basalts and contemporary felsic, mafic and ultramafic intrusions [10–15]. Basalts as the predominant component of ELIP could be divided into two groups: high-Ti ($\text{Ti}/\text{Y} > 500$) and low-Ti ($\text{Ti}/\text{Y} < 500$) basalts [13]. Three ELIP zones including inner, intermediate, and outer zones were recognized (Figure 1A) based on the extent of erosion of the pre-ELIP eruption Maokou Formation (with limestone-dominated compositions) of Middle Permian age in SW China [11].

Within the inner zone of the ELIP is the Kangdian Oldland comprising a sequence of Emeishan basalts, which existed until the Middle Triassic [11]. In the eastern ELIP, the Emeishan basalts unconformably overlie the Maokou Formation of Middle Permian age while the ELIP basalts are, in turn, overlain by the Late Permian Xuanwei and Longtan formations (Figure 1B) [11]. During the Late Permian, the ELIP and associated volcanism and hydrothermal activity controlled the development of coal-bearing strata in SW China, not only in serving the source for the peat-accumulation process, but also the distribution of peat-mire sites (*i.e.*, peat-mires located in the middle and outer zones of ELIP) [2].

The Nb(Ta)-Zr(Hf)-REE-Ga polymetallic mineralization is found in the intermediate ELIP zone and is located in the lowest Xuanwei Formation in eastern Yunnan Province (Figures 1 and 2) [1]. The Xuanwei Formation is a continental formation containing the major coal-bearing strata of Late Permian age in eastern Yunnan Province, southwest China [1,16–19] and is mainly derived from erosion of the Kangdian Oldland in the central ELIP [2,15,20–22].

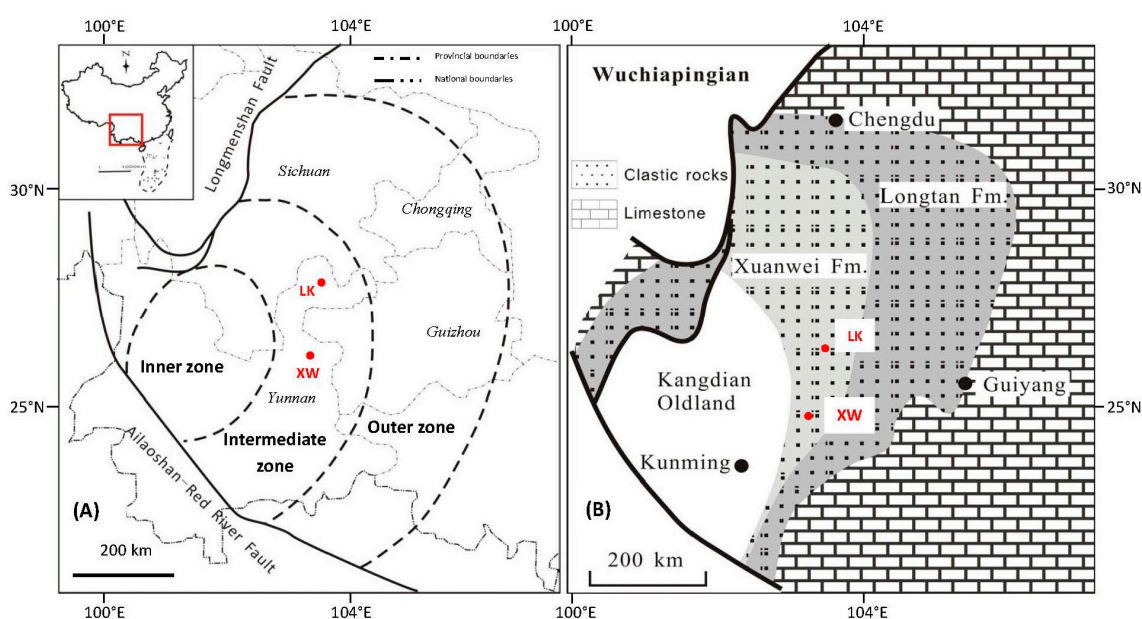


Figure 1. Geological setting during Late Permian in southwest China, showing the location of Nb-Zr-REE-Ga mineralization. (A) Schematic map showing the inner, intermediate and outer zones of the Emeishan Large Igneous Province. (B) Paleogeography map showing the distribution of terrestrial Xuanwei Formation and transitional Longtan Formation during the Wuchiapingian in SW China. The red spots indicate the localities of the two studied drill holes (XW and LK). Figure 1 is modified from [20].

3. Samples and Analytical Procedures

A total of 39 samples, corresponding to the high anomalies on natural gamma log curves, were collected from Nos. XW and LK drill holes in eastern Yunnan Province, SW China. These samples were identified as X-1 to X-17, and L-1 to L-22 from top to bottom, respectively (Figure 2). The samples are mainly mudstone, and in a few cases sandstones. Calcite veins, pyrite grains, hematite, and plant fragments are commonly observed in hand-specimens.

Polished thin-sections and polished block samples were prepared from selected samples for optical and scanning electron microscopic observations. All samples were then crushed and milled to pass 200-mesh for bulk X-ray diffraction (XRD) analysis (Rigaku, Tokyo, Japan). Bulk-XRD analysis was performed using a Rigaku D/max 2500 pc powder diffractometer equipped with Ni-filtered Cu-K α radiation and scintillation detector in China University of Mining and Technology (Beijing). Each XRD pattern was recorded over a 2θ interval of 2.6° – 70° , with a step size of 0.02° . Quantitative analysis

for each mineral phase was carried out by a commercial XRD interpretation software Siroquant™ (Sietronics Pty Ltd., Belconnen, ACT, Australia).

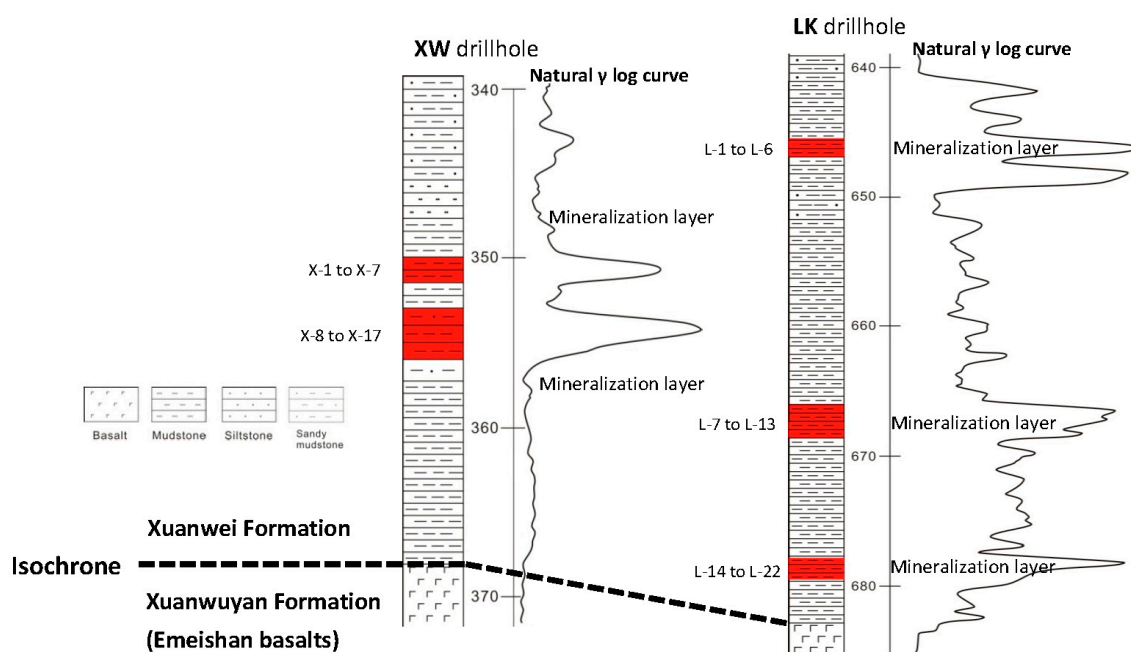


Figure 2. Stratigraphic sections of the XW and LK drill holes. The red areas indicate the sampling locations.

Modes of occurrence of minerals were investigated using a FEI Quanta™ 650 FEG scanning electron microscope (SEM, EDAX Inc., Mahwah, NJ, USA) in China University of Mining and Technology (Beijing), China and a Hitachi S3400-X/I SEM (Hitachi, Tokyo, Japan) at the University of New South Wales, Australia. The selected polished thin-sections and sample blocks were carbon-coated before SEM observation. The Quanta SEM worked with a beam voltage of 20.0 kV, working distance ~10 mm, and a spot-size of 5.5 while, for the Hitachi-S3400 X/I, the accelerating voltage was 20 kV, and the beam current was 40–60 mA during SEM operation.

Sample powders were mixed with water and then settled for approximately 2 h for acquiring clay-bearing suspensions. Suspended clay particles were concentrated through centrifuging (8 min at 2500 rpm). The concentrated clay fractions were placed evenly on glass slides. Three XRD runs were performed on each slide after air-drying, exposure to ethylene-glycol vapor (more than 24 h) and heating to 400 °C for 1 h using a PANalytical Empyrean II XRD (Co-K α ; PANalytical Ltd., Almelo, The Netherlands) at the University of New South Wales, Australia, with tube voltage of 45 kV and current of 40 mA.

4. Results

4.1. Mineral Phases and Clay Species in the Studied Sample

Mineralogical compositions based on powder XRD and Siroquant analyses in the studied samples are given in Table 1. Mineral phases in this study include clay minerals, quartz, anatase, calcite, siderite, hematite, albite, and florencite (Table 1; Figure 3). Pyrite occurring either as discrete grains or as veinlets was commonly observed but its content was generally below the detection limit of XRD or Siroquant techniques.

Table 1. Mineral contents (%) in the studied samples, and the estimated percentages of smectite layers *i.e.*, S (%) and Reichweite values for I/S. “-” means below the detection limit of Siroquant analysis.

Samples	I/S	Kaolinite	Berthierine	Quartz	Anatase	Calcite	Florencite	Siderite	Albite	Hematite	Total Clay	S (%)	Reichweite Value
X-1	15.2	42.6	17.5	22.8	1.9	-	-	-	-	-	75.3	35	R1
X-2	23.5	57.7	12.3	5.2	1.4	-	-	-	-	-	93.5	35	R1
X-3	27.0	56.5	4.7	10.3	1.6	-	-	-	-	-	88.2	35	R1
X-4	51.9	28.4	4.3	12.8	1.6	0.9	-	-	-	-	84.6	30	R1
X-5	35.0	35.4	18.4	8.8	2.0	0.5	-	-	-	-	88.8	30	R1
X-6	22.8	39.7	22.9	13.6	1.0	-	-	-	-	-	85.4	30	R1
X-7	54.2	12.9	-	28.0	1.3	3.7	-	-	-	-	67.1	25	R1
X-8	45.5	29.6	11.6	11.8	0.6	0.9	-	-	-	-	86.7	30	R1
X-9	54.5	24.2	5.1	15.7	0.5	-	-	-	-	-	83.8	30	R1
X-10	43.9	28.2	10.1	16.9	0.9	-	-	-	-	-	82.2	30	R1
X-11	78.4	3.9	2.1	15.5	0.2	-	-	-	-	-	84.4	25	R1
X-12	75.9	1.2	1.5	19.8	-	1.5	-	-	-	-	78.6	25	R1
X-13	69.6	2.6	0.7	26.2	0.8	-	-	-	-	-	72.9	25	R1
X-14	75.7	1.2	3.9	19.2	-	-	-	-	-	-	80.8	25	R1
X-15	77.6	4.4	2.0	16.0	-	-	-	-	-	-	84.0	25	R1
X-16	57.8	9.0	6.0	14.1	0.2	12.3	-	0.7	-	-	72.7	25	R1
X-17	45.1	19.2	1.4	32.3	1.1	0.8	-	-	-	-	65.7	20	R1
L-1	31.1	13.4	19.1	33.5	2.3	-	0.5	-	-	-	63.6	20	R1
L-2	52.9	0.9	16.6	25.3	1.5	2.3	0.5	-	-	-	70.4	20	R1
L-3	56.1	1.5	6.1	28.0	0.9	7.0	0.3	-	-	-	63.7	20	R1
L-4	66.3	5.3	1.4	15.2	1.1	10.0	0.6	-	-	-	73.0	20	R1
L-5	20.6	8.1	10.5	52.2	-	7.9	0.7	-	-	-	39.2	20	R1
L-6	74.0	10.0	9.9	0.8	5.3	-	-	-	-	-	93.9	20	R1
L-7	28.0	4.1	31.9	23.6	1.4	-	-	11.1	-	-	64.0	20	R1
L-8	65.9	4.9	15.5	12.2	1.5	-	-	-	-	-	86.3	20	R1
L-9	58.7	5.3	4.3	30.8	0.9	-	-	-	-	-	68.3	20	R1
L-10	66.6	7.7	4.9	19.1	1.8	-	-	-	-	-	79.2	20	R1
L-11	33.3	-	51.9	0.4	4.5	-	0.1	6.4	-	3.3	85.2	20	R1
L-12	54.1	-	32.3	0.8	6.0	-	-	3.7	-	3.1	86.4	20	R1
L-13	69.0	11.0	6.4	7.4	2.3	-	0.5	-	-	3.5	86.4	25	R1
L-14	53.6	17.3	16.8	4.1	4.7	-	0.7	-	-	2.7	87.7	20	R1
L-15	71.7	5.9	8.8	9.1	1.8	-	-	-	-	2.7	86.4	20	R1
L-16	69.5	8.7	3.3	13.8	0.8	-	0.7	-	-	3.1	81.5	20	R1
L-17	65.5	9.8	0.4	23.3	1.0	-	-	-	-	-	75.7	20	R1
L-18	53.2	8.0	15.8	20.3	2.7	-	-	-	-	-	77.0	20	R1
L-19	41.9	10.4	9.2	30.6	0.1	-	0.5	-	7.3	-	61.5	20	R1
L-20	64.9	3.2	13.1	15.1	3.1	-	0.7	-	-	-	81.2	20	R1
L-21	44.1	8.6	17.9	28.1	0.8	-	0.5	-	-	-	70.6	20	R1
L-22	59.0	8.3	14.2	17.4	1.1	-	-	-	-	-	81.5	15	R3

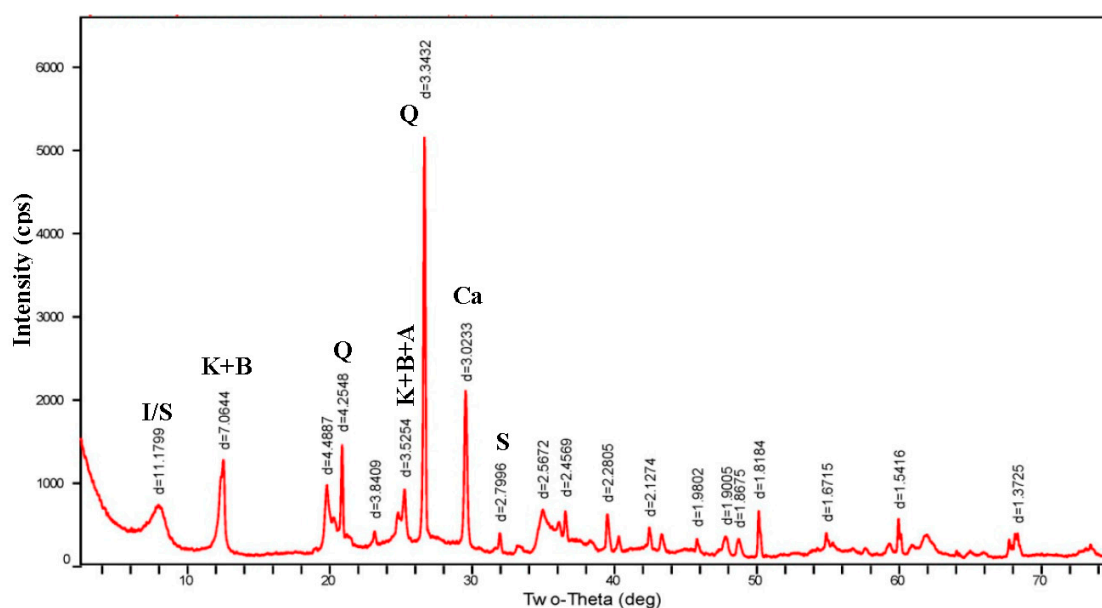


Figure 3. XRD of a selected sample (X-16). Abbreviations in the figure indicate the minerals identified, such as I/S: mixed layer illite/smectite; K: kaolinite; B: berthierine; Q: quartz; A: anatase; Ca: calcite; and S: siderite.

The clay species were further identified by the analyses of the three XRD runs on air-dried, Ethylene Glycol (EG)-solvation and heated specimens. Clay minerals identified in the studied samples comprise mixed layer illite/smectite (I/S), kaolinite, and berthierine (Figures 3 and 4). I/S has been recognized by comparing the bulk-XRD pattern (and the air-dried patterns) to XRD patterns of the ethylene-glycol treated and heated specimens. The characteristic broad peaks of mixed layer I/S are located at $11 \text{ \AA} \pm$ in the bulk and air-dried oriented patterns, split into two peaks at $12 \text{ \AA} \pm$ and $9 \text{ \AA} \pm$ after EG solvation, and move towards 10 \AA for the heated sample (Figures 3 and 4) [23]. Kaolinite is distinguished by the 7.2 \AA and 3.58 \AA peaks in the bulk and air-dried patterns which do not change in the patterns for the EG specimen while in the heated specimen, these peaks reduce or disappear [23]. Berthierine, which has a similar structure to kaolinite and similar chemical composition to chlorite, is distinguished by a lack of 14 \AA reflections and a 7 \AA basal spacing in the XRD patterns [24–26]. In the XRD pattern, the $d(001)$ intensity of berthierine is slightly lower than that of kaolinite (Figure 4). Kaolinite may mask berthierine in the bulk XRD patterns owing to the proximate (001) and (002) reflections of these two minerals; however, they can be identified from each other in the air-dried oriented pattern (Figure 4). The $d(001)$ reflection of berthierine will considerably reduce after being heated (Figure 4) [27].

I/S in all the studied samples was identified as ordered according to the position of split peaks, as well as the presence of the basal peak at 27 \AA in the EG-solvation specimens [23]. The percentages of smectite layers of I/S *i.e.*, S (%) in the studied samples were estimated based on the d -spacing values of I/S in EG-XRD patterns, as listed in Table 1. Apparently, S (%) in samples from XW drill hole (25%–35%) is higher than those from LK drill hole (15%–20%). I/S in most of the samples are identified as R1 ordered with only one R3 I/S in L-22 (Table 1; R: Reichweite parameters; [28]).

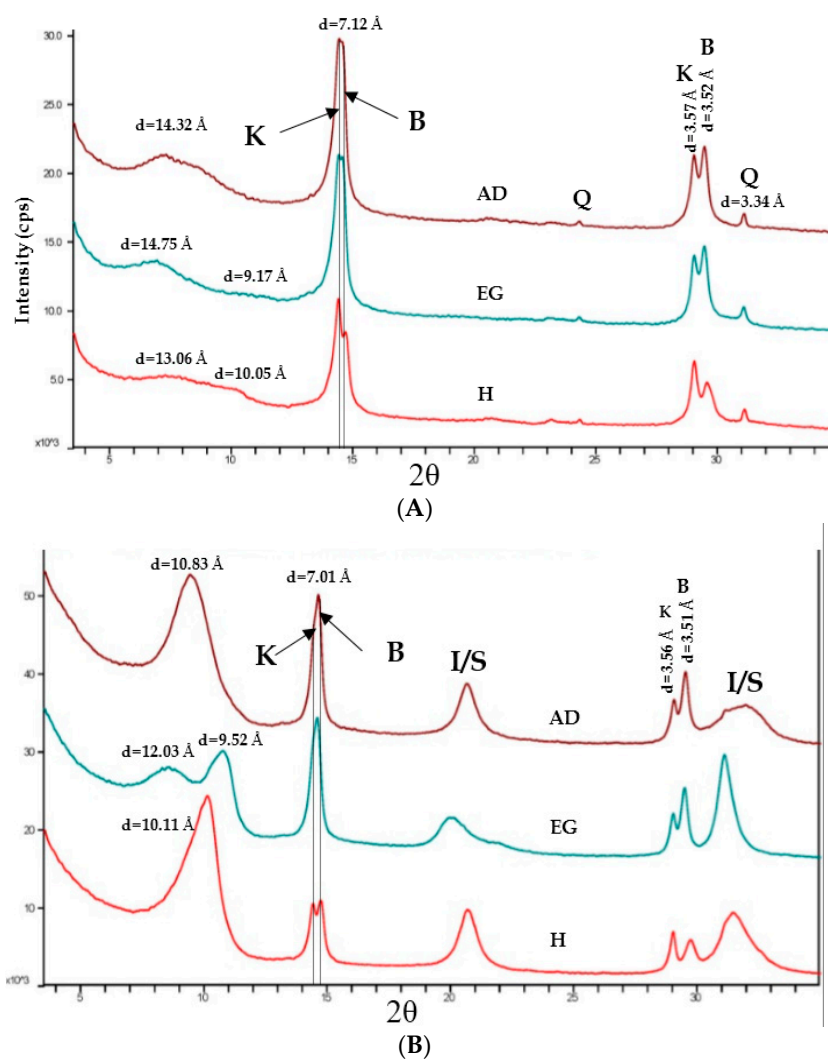


Figure 4. XRD patterns for air-dried, EG-solvation, and heated clay fractions of selected samples (A) X-2 and (B) L-19. Abbreviations are same as in Figure 3. AD: air-dried; EG: ethylene glycol saturated; H: heated.

4.2. Modes of Occurrence of Clay Minerals

Clay minerals in this study show various modes of occurrence. Mixed layer illite/smectite mainly occurs as groundmass for other minerals (not only non-clay minerals, but also kaolinite and berthierine; Figure 5). In some cases, I/S has a needle-/lath-like shape (Figure 6A) and is also found in plant cells (Figure 6B) probably indicating an authigenic origin.

Berthierine in this study shows pale red-yellowish discrete particles within I/S matrix under the microscope (Figure 5A). The berthierine particles are usually sharp-cornered and elongated in shape and vary in length from 50 μm to more than 300 μm (Figures 5A and 6C,D). Under SEM, berthierine not only occurs as angular particles (Figure 6C,D), but also colloidal infillings in plant cells coexisting with I/S or quartz (Figure 6B,E). In a few cases, berthierine precipitated along the cracks of vermicular kaolinite (Figure 6F). In Figure 6C,D, berthierine grains were eroded with I/S filling within the cavities or surrounding the remnant berthierine particles.

Vermicular kaolinite is commonly found under both the microscope and SEM. Vermicular kaolinite shows yellowish color under the cross-polarized light under SEM, and in some cases, kaolinite was altered to colloidal berthierine along the margins of kaolinite crystal (Figures 5B and 6F).

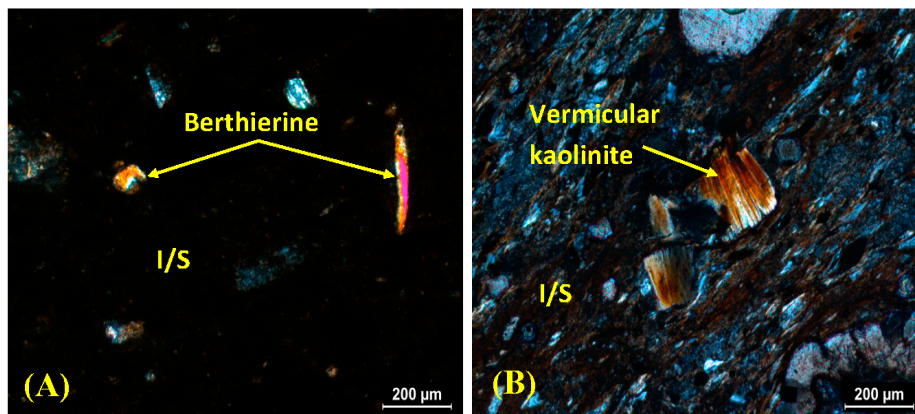


Figure 5. Microscopic observations of the studied samples (cross-polarized light). (A) Volcanic shard-like berthierine particles (X-17); (B) Vermicular kaolinite (L-11).

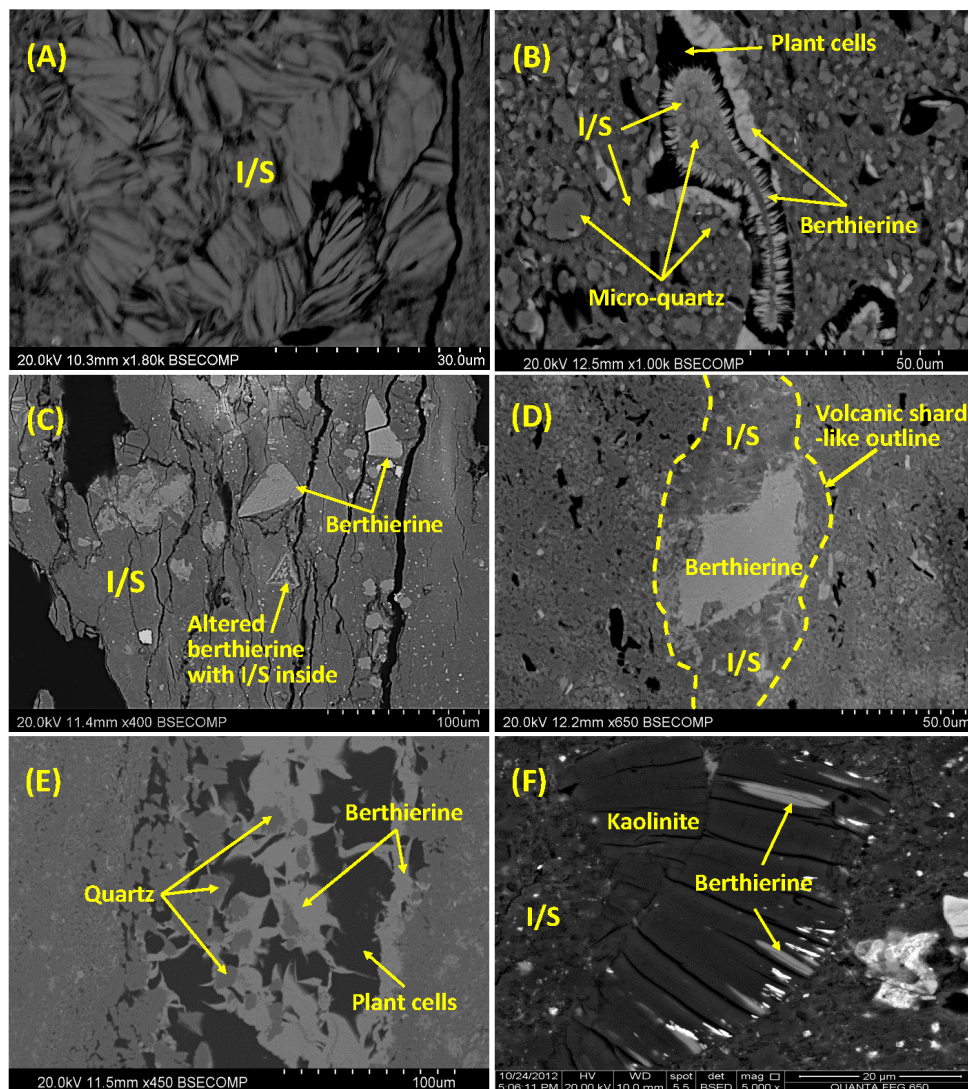


Figure 6. Back-scattered electron images of clay minerals. (A) Authigenic lath-like I/S (X-2); (B) Berthierine and I/S within plant cell (black areas), and micro-quartz particles (X-1); (C) Berthierine particles (X-2); (D) I/S surrounding berthierine (L-18); (E) Quartz coexisting with berthierine within plant cells (L-5); (F) berthierine within fractures of vermicular kaolinite (X-10).

4.3. Abundances of Clay Minerals

Clay minerals are dominant in almost all the studied samples (total clay: 65.7%–93.5%, mean 80.9% in XW#; 39.2%–93.9%, mean 75.6% in LK#; Table 1), followed by quartz (XW#: 5.2%–32.3% and LK#: 0.4%–52.2%; Table 1) and anatase. Calcite is commonly found under both micro- and macro-observations and in a few cases, the content of calcite is up to 12.3% (XW-16; Table 1). Siderite, albite, and hematite are only rarely found in LK drill holes. Trace REE-bearing phosphate florencite was also discovered in some samples from LK drill holes.

Regarding the clay minerals, I/S is more abundant than kaolinite and berthierine, for example the content of I/S in XW drill holes ranges from 15.2% to 78.4%, averaging 50.6% while in LK drill holes, this value is from 20.6% to 74%, with an average of 54% (Table 1). In general, samples from XW drill hole contain more kaolinite (1.2%–57.7%; Table 1) than those from LK drill hole (bdl–17.3%; bdl: below detection limit; Table 1). In contrast, berthierine seems more abundant in LK drill hole (0.4%–51.9%; Table 1) than in XW drill hole (bdl–22.9%; Table 1).

5. Discussions

5.1. Volcanic Ash Control on Modes of Occurrence of Clay Assemblages

Based on the petrologic, mineralogical, geochemical, and geophysical studies by Dai, *et al.* [1], the Nb-Zr-REE-Ga-mineralized horizons represent argillized tuffs originated from alkaline volcanic ashes. This is mainly because we have found typical tuffaceous instead of sedimentary textures, and shard-like and euhedral magmatic high-temperature minerals within the Nb-Zr-REE-Ga-mineralized samples under both the microscope and SEM [1,2]. These high-temperature magmatic mineral phases (such as beta-quartz, euhedral apatite, and zircon *etc.*) with high-T cracks, embayments, and sharp-edged outlines were not hydraulically sorted debris which usually have rounded morphologies. It is believed that the Nb-Zr-REE-Ga-mineralized samples and the contained elevated rare metals were derived from alkaline volcanic ash [1]. Natural gamma log data from more than 300 drill holes have shown that the Nb-Zr-REE-Ga-mineralized beds with high positive natural gamma anomalies have a continuous lateral extent across the lowest Upper Permian strata of SW China [1,2]. The widespread Nb-Zr-REE-Ga-mineralized beds with a uniform geochemistry and mineralogy are also indicative of a volcanic tuff deposition [1,2]. In some cases, the abrupt contact between the Nb-Zr-REE-Ga-mineralized rocks and the wall rocks may also be caused by the volcanic-ash origin of the former [1]. These Nb-Zr-REE-Ga-mineralized beds in the lowest Upper Permian strata, have a temporal link to the ~260 Ma Emeishan large igneous province and are the results of waning activity of Emeishan mantle plume [2,29]. The glass-rich volcanic ashes would be an ideal precursor for the clay minerals [30]. In this study, the volcanic origin of the studied samples is also reflected by the modes of occurrence of the clay minerals.

Berthierine is one of the dominant minerals in the Nb(Ta)-Zr(Hf)-REE-Ga ore deposit [1] and has been found within Paleogene and Late Triassic coals of Japan [31]; however, in the Late Permian coals from southwest China, berthierine is not widely reported while an Fe-rich chlorite (*i.e.*, chamosite which is characterized by the 14 Å on XRD pattern; cf. Dai and Chou [32]) is commonly found [32–35]. Berthierine in this study is mainly found occurring as individual angular particles although a small proportion of authigenetic colloidal berthierine can be observed as well. Such berthierine with various irregular shapes (*cf.* Figures 5 and 6) rather than the rounded shape or lumps following the bedding planes indicates that it had not been sorted by weathering and transportation process but is most likely to be transformed from the volcanic glass shards transported by air [36]. Under a microscope, shard-like berthierine occurring discretely within the matrix is also similar to the texture of a volcanic tuff (Figure 5A).

Kaolinite is a common mineral phase in coals and the intra-seam parting tonstein, generally a dominant clay species within clay assemblages in coal, probably due to its stability in low-pH peat mire which contains humic acid released from organic matter at early stage of coal-forming

process [16,30,37]. Deconinck *et al.* [38] generated that kaolinite may be derived either from volcanic ashes or from detrital materials. Additionally, Ward [39] suggested that authigenic kaolinite occurring in pores and cavities in coal may be precipitated from solutions. The well-crystallized vermicular texture of kaolinite crystal is believed as volcanic ash-altered product in oxygen-depleted conditions and would occur in the volcanic horizons within coal-forming peat mires [30,34,40,41] or marine environments [38]. In this study, the microscopic and SEM observations revealed the presence of widespread vermicular aggregates of kaolinite is widespread (Figures 5B and 6F), indicating these kaolinite crystals were of authigenic origin and formed *in situ* through alteration of volcanic glass [38].

I/S is also a common mineral in coal [39] and in general, I/S is not the dominant minerals [42]. In fact, the clay fractions in this study, especially kaolinite and I/S have been described within volcanic-ash originated depositions of coal-bearing strata [30]. I/S has been reported in most Mesozoic bentonites [30], the lower Cretaceous bentonites, British Columbia [43–45], Oxfordian bentonites from the Subalpine Basin, Turonian bentonites of France [46], and Ordovician Kinnekulle K-bentonites, France [47]. Furthermore, I/S-enriched Late Permian coals were reported in the Changxing Mine, eastern Yunnan, southwest China (closely located to the drill holes present in this study) [42]. Volcanic ashes falling into the peat mire would transform to smectite; I/S was probably derived from illitisation of volcanic ashes originated smectite during burial diagenesis [30]. Based on the occurrence that I/S coexists with berthierine within the outline of volcanic glass (Figure 6D), it is inferred that both I/S and berthierine were derived from alteration of volcanic glass.

In addition to the volcanic ashes, hydrothermal fluids may have also participated in the formation of clay minerals. The minerals in the plant cells (Figure 6B,E), along with the rare metal-bearing minerals (including hydrothermal REE-bearing phosphate and carbonate, and Nb-bearing anatase *etc.*) occurring within pores and cavities of clay minerals [2] indicate that these minerals are authigenic origin derived from re-deposition of free-ions leached from volcanic ashes by hydrothermal fluids [2]. Clay minerals may have grown from hydrothermal solutions enriched in Si, Al, Fe, K, *etc.* by dissolution of volcanic ashes (including volcanic minerals and glasses).

5.2. Implications for Paleo-Diagenetic Temperature

The clay minerals in this study, particularly I/S, are sensitive to thermal conditions, thus their characteristics can be used to estimate the paleo-diagenetic temperatures during the burial process [31,38,48–50]. Factors affecting formation of ordered I/S include temperature, fluid chemistry, time, source material composition, and permeability of the host rock [48,51,52]. In the present study, the latter three factors are unlikely to be the main controls on the ordering of I/S because most of the studied samples are mudstones derived from the same phase of alkaline volcanism with same magma source in the earliest Late Permian [1,2]. Temperature and fluid chemistry thus should be the dominant factors that would have influenced the formation of I/S in this study. Many studies have focused on the diagenetic temperature during the burial process, using the evolution of smectite illitization (especially the percentages of smectite layers within I/S) [48,50,53–55]. In the XRD patterns for the EG-saturated clay fractions, as smectite layers decrease in I/S, the peaks at 9 Å, as well as peaks at 5 Å, become sharp and narrow showing a trend towards illite and indicating a progressive increment in temperature (Figure 7). It has been suggested that the temperature that reflects the appearance of R1 I/S during the smectite illitization process is generally around 100 °C while the transition temperature from R1 to R3 I/S can be up to *ca.* 180 °C [48,50,53–55]. In this study, most of the studied samples have the R1 ordered I/S, except for only one sample that has the R3 ordered I/S (Table 1) indicating that the paleo-diagenetic temperature for the studied samples could have been up to 180 °C but for most of the samples, this value ranges from 100 to 180 °C.

Considering the influence of fluids, it is interesting to note that in the samples from XW drill hole, especially in the lower bed (X-11 to X-16), the contents of kaolinite and berthierine tend to decrease from X-10 to (X-11 to X-16), and then increase in X-17 (Table 1). In addition to the sharp decrease of contents of kaolinite and berthierine, the ordering of their structure also starts to become poor (reflected

by the broad peaks at 7 and 3.5 Å), along with an increase in the contents and ordering of I/S in X-11 to X-16 (Table 1; Figures 3, 4 and 7). The changes in contents and crystal ordering may reflect the re-forming of clay minerals under conditions that allow for the poorly-ordered kaolinite and berthierine to form [51]. While in the presence of K released from volcanic ashes, the conversion of well-ordered kaolinite to disordered kaolinite and I/S would have happened under hydrothermal conditions [51]. The colloidal/infilling minerals which were precipitated from hydrothermal fluids revealed in part 4 and a previous study [2] suggest that hydrothermal fluids influenced the studied samples during diagenesis. Accordingly, a reaction mechanism that the kaolinite, as well as berthierine (which has a similar structure to kaolinite [26]) had transformed into I/S under hydrothermal conditions is possible. Such a transformation was estimated to have occurred in a thermal metamorphism environment at a temperature around 225–250 °C [51]; however, as for this study, if the temperature had reached 225 °C, the corresponding I/S in these samples should be R3 ordered. In contrast, as revealed in Table 1, I/S in these samples R1 is still ordered with a slight decrease of 5% smectite layers within I/S. Therefore, such a high temperature seems improbable for the present study.

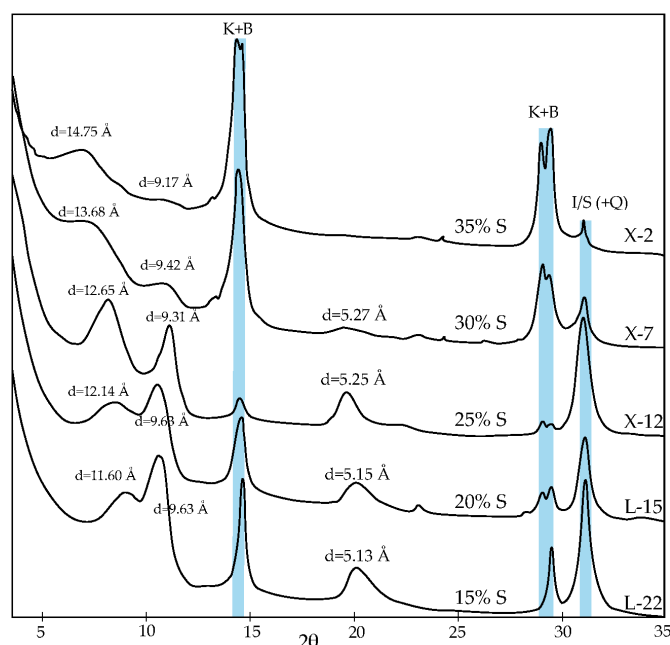


Figure 7. XRD patterns for EG-solvation slides with S (%) = 15, 20, 25, 30, 35, respectively. Blue bars indicate the synthetic peaks at 7, 3.5 and 3.3 Å. Abbreviations are the same as Figure 3.

Berthierine is another temperature-sensitive mineral which remains stable under a wide range of temperatures but generally lower than 200 °C [56]. Although in some cases, the transformation of berthierine to chamosite during diagenesis at lower temperatures was reported (below 70 °C when accompanied by organic matter) [31,56,57], that berthierine could have formed at higher temperature was revealed by Iijima and Matsumoto [31], who suggested the formation temperature of berthierine in coal to be 65–150 °C while the alteration temperature of berthierine higher than 160 °C. A similar crystallization temperature of berthierine (150 °C) was also reported by Rivas-Sanchez, *et al.* [25]. If we adopt Iijima and Matsumoto's [31] viewpoint to estimate the paleotemperature of the coal-hosted Nb-Zr-REE-Ga mineralization, since no traces of berthierine transforming to chamosite were found (*i.e.*, no 14 Å were found in XRD patterns) in this study, the paleotemperature should be below 160 °C.

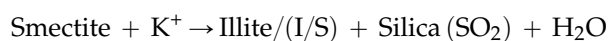
Overall, temperature should be the primary control on the formation of I/S with in some cases, the hydrothermal activity as a secondary control. It is reasonable to estimate that the paleo-diagenetic temperature for the studied samples was 100–160 °C, with one case up to 180 °C. The distribution

patterns of rare earth elements (e.g., negative Eu anomalies) in the ore beds also showed that the temperature is lower than 200 °C [58].

5.3. Origin of the Micro-Crystalline Quartz Associated with Mixed Layer I/S

Microcrystalline quartz with sizes generally less than 10 µm (mostly <5 µm; Figure 6B) was observed in this study. These very fine quartz grains/cements were found isolated and surrounded by a clay matrix (mainly I/S; Figure 6B). It is unlikely that this micro-quartz formed via mechanical transportation as quartz of a detrital origin is generally in silt- to sand-size particles [59]. Additionally, the pyroclastic quartz in the Nb-Zr-REE-Ga mineralization was reported as large angular particles (>50 µm) [1]. These individual micro-crystalline quartz particles are, therefore, most likely authigenic rather than detrital or pyroclastic in origin. The authigenic ultrafine quartz grains (around 10 µm) were also found in Late Permian coal from Xuanwei, east Yunnan Province, SW China [32] and the Early Cretaceous Wulantuga coal, Inner Mongolia, North China [59].

It has been suggested that illitization of smectite releases Si and involves addition of K [51,60–63]. The excess released Si in solutions (e.g., pore water) may precipitate locally as authigenic micro-crystalline quartz coexisting with the neoformed I/S [62,63]. A simplified reaction process would be:



Peltonen *et al.* [62] suggested that the sources of smectite and potassium will govern the amount of Si released in such a reaction. In this study, as the studied samples are of pyroclastic origin [1], the smectite in the above equation would be from the alteration of volcanic glasses while volcanic ash-accompanied K-feldspar could have provided K for the illitization of smectite. Another factor limiting the precipitation of quartz from Si-solutions is the permeability of the host rocks, for example, Si-fluids would migrate easier from sandstone (high permeability) than from mudstone (low permeability) [63]. In this study, the low permeability of the studied samples (*i.e.*, mostly mudstones), restricting the diffusion of fluids that contain Si released from illitization of smectite, could also have favored the *in situ* deposition of quartz.

With all the above in mind, we assume that the illitization of smectite during diagenesis may have released significant amounts of SiO₂ into solutions first; then due to the low permeability of the studied mudstones, the SiO₂-rich solutions resulted in the formation of the micro-crystalline quartz *in situ* as grains near the I/S. As the progressive illitization of smectite proceeded during diagenesis, SiO₂ was continuously released to form the high silica saturated solutions favoring the further continuous crystallization and growth of the micro-quartz to become macro-crystalline quartz cements or aggregates [63]. Such a process may also be the cause of high quartz contents in the studied samples (Table 1).

6. Conclusions

- (1) The clay minerals in the Nb(Ta)-Zr(Hf)-REE-Ga mineralized beds mainly comprise I/S, kaolinite, and berthierine. Generally, I/S is the most abundant species among the clay minerals while the contents of kaolinite and berthierine vary greatly. Angular berthierine particles and vermicular kaolinite occur within the I/S groundmass, while a small proportion of berthierine occurs as colloidal infillings coexisting with I/S in plant cells or in the fractures of vermicular kaolinite.
- (2) The modes of occurrence of kaolinite and berthierine verify a volcanic origin for the studied samples. Vermicular kaolinite and the angular berthierine are probably *in situ* alteration products of volcanic ashes. I/S is the product of illitization of volcanic-ash originated smectite.
- (3) Indicated by the presence of berthierine and the ordering of the I/S, the paleo-diagenetic temperature reached *ca.* 180 °C, but was generally within 100–160 °C.
- (4) The authigenic micro-crystalline quartz coexisting with I/S is probably the result of illitization of smectite during the diagenetic process.

Acknowledgments: This research was supported by the National Key Basic Research Program of China (No. 2014CB238902), the National Natural Science Foundation of China (Nos. 41420104001 and 41272182), and the Program for Changjiang Scholars and Innovative Research Team in University (IRT13099). We would like to thank Colin Ward and David French from the University of New South Wales, Australia for their help in clay mineral identification and quantification, and Xisheng Lin from the Research Institute of Petroleum Exploration & Development, China for analysis of mixed layer illite/smectite. Joanne Wilde from the University of New South Wales, Australia is thanked for preparing the polished thin-sections for this study.

Author Contributions: All co-authors participated in the work of this study. Lixin Zhao carried-out the clay mineralogy analyses and interpreted mineralogical data under the supervision of Ian Graham. Shifeng Dai collected the samples in the field and has carried-out the field investigation. Ian Graham and Shifeng Dai helped to design the research and structure of the manuscript, as well as the correcting the English language of this manuscript. Peipei Wang conceived and determined the ordering of mixed layer I/S.

Conflicts of Interest: The authors declare no conflict of interest.

References

1. Dai, S.; Zhou, Y.; Zhang, M.; Wang, X.; Wang, J.; Song, X.; Jiang, Y.; Luo, Y.; Song, Z.; Yang, Z.; Ren, D. A new type of Nb(Ta)-Zr(Hf)-REE-Ga polymetallic deposit in the Late Permian coal-bearing strata, eastern Yunnan, southwestern China: Possible economic significance and genetic implications. *Int. J. Coal Geol.* **2010**, *83*, 55–63. [[CrossRef](#)]
2. Dai, S.; Chekryzhov, I.Y.; Seredin, V.V.; Nechaev, V.P.; Graham, I.T.; Hower, J.C.; Ward, C.R.; Ren, D.; Wang, X. Metalliferous coal deposits in East Asia (Primorye of Russia and South China): A review of geodynamic controls and styles of mineralization. *Gondwana Res.* **2016**, *29*, 60–82. [[CrossRef](#)]
3. Dai, S.; Ren, D.; Chou, C.-L.; Finkelman, R.B.; Seredin, V.V.; Zhou, Y. Geochemistry of trace elements in Chinese coals: A review of abundances, genetic types, impacts on human health, and industrial utilization. *Int. J. Coal Geol.* **2012**, *94*, 3–21. [[CrossRef](#)]
4. Dai, S.; Ren, D.; Zhou, Y.; Seredin, V.V.; Li, D.; Zhang, M.; Hower, J.C.; Ward, C.R.; Wang, X.; Zhao, L.; *et al.* Coal-hosted rare metal deposits: Genetic types, modes of occurrence, and utilization evaluation. *J. China Coal Soc.* **2014**, *39*, 1707–1715. (In Chinese)
5. *Geology Mineral Industry Standard of P.R. China: Specifications for Rare Metal Mineral Exploration*; DZ/T 0203-2002; Geological Press: Beijing, China, 2002. (In Chinese)
6. Committee of National Resources. *Reference Handbook for Mineral Industry Requirements*; Geological Press: Beijing, China, 2010. (In Chinese)
7. *Geology Mineral Industry Standard of P.R. China: Specifications for Rare Earth Mineral Exploration*; DZ/T 0204-2002; Geological Press: Beijing, China, 2002. (In Chinese)
8. Zhou, Y. The synsedimentary alkalinity-volcanic ash derived tonsteins of early Longtan age in southwestern China. *Coal Geol. Explor.* **1999**, *27*, 5–9. (In Chinese)
9. Zhou, Y.; Bohor, B.F.; Ren, Y. Trace element geochemistry of altered volcanic ash layers (tonsteins) in Late Permian coal-bearing formations of eastern Yunnan and western Guizhou provinces, China. *Int. J. Coal Geol.* **2000**, *44*, 305–324. [[CrossRef](#)]
10. Ali, J.R.; Fitton, J.G.; Herzberg, C. Emeishan large igneous province (SW china) and the mantle-plume up-doming hypothesis. *J. Geol. Soc.* **2010**, *167*, 953–959. [[CrossRef](#)]
11. He, B.; Xu, Y.-G.; Chung, S.-L.; Xiao, L.; Wang, Y. Sedimentary evidence for a rapid, kilometer-scale crustal doming prior to the eruption of the Emeishan flood basalts. *Earth Planet. Sci. Lett.* **2003**, *213*, 391–405. [[CrossRef](#)]
12. Shellenutt, J.G. The Emeishan large igneous province: A synthesis. *Geosci. Front.* **2014**, *5*, 369–394. [[CrossRef](#)]
13. Xu, Y.; Chung, S.-L.; Jahn, B.-M.; Wu, G. Petrologic and geochemical constraints on the petrogenesis of Permian-Triassic Emeishan flood basalt in southwestern China. *Lithos* **2001**, *58*, 145–168. [[CrossRef](#)]
14. Chung, S.L.; Jahn, B.M. Plume-lithosphere interaction in generation of the Emeishan flood basalts at the Permian-Triassic boundary. *Geology* **1995**, *23*, 889–892. [[CrossRef](#)]
15. Xu, Y.; He, B.; Luo, Z.; Liu, H. Large igneous provinces in China and mantle plume: An overview and perspective. *Bull. Mineral. Petrol. Geochem.* **2013**, *32*, 25–39. (In Chinese)
16. China Coal Geology Bureau. *Sedimentary Environments and Coal Accumulation of Late Permian Coal Formation in Western Guizhou, Southern Sichuan and Eastern Yunnan, China*; Chongqing University Press: Chongqing, China, 1996. (In Chinese)

17. Feng, Z.; Yang, Y.; Jin, Z.; Li, S.; Bao, Z. *Lithofacies Paleogeography of Permian of South China*; China University of Petroleum Press: Dongying, China, 1997. (In Chinese)
18. Wang, S.; Yin, H. *Study in Terrestrial Permian-Triassic Boundary in Eastern Yunnan and Western Guizhou*; China University of Geoscience Press: Wuhan, China, 2001. (In Chinese)
19. Zhang, Z.; Yang, X.; Li, S.; Zhang, Z. Geochemical characteristics of the Xuanwei Formation in West Guizhou: Significance of sedimentary environment and mineralization. *Chin. J. Geochem.* **2010**, *29*, 355–364. [[CrossRef](#)]
20. He, B.; Xu, Y.-G.; Huang, X.-L.; Luo, Z.-Y.; Shi, Y.-R.; Yang, Q.-J.; Yu, S.-Y. Age and duration of the Emeishan flood volcanism, SW China: Geochemistry and SHRIMP zircon U–Pb dating of silicic ignimbrites, post-volcanic Xuanwei Formation and clay tuff at the Chaotian section. *Earth Planet. Sci. Lett.* **2007**, *255*, 306–323. [[CrossRef](#)]
21. He, B.; Xu, Y.-G.; Zhong, Y.-T.; Guan, J.-P. The Guadalupian-Lopingian boundary mudstones at Chaotian (SW China) are clastic rocks rather than acidic tuffs: Implication for a temporal coincidence between the end-Guadalupian mass extinction and the Emeishan volcanism. *Lithos* **2010**, *119*, 10–19. [[CrossRef](#)]
22. Xu, Y.; He, B.; Chung, S.-L.; Menzies, M.A.; Frey, F.A. Geologic, geochemical, and geophysical consequences of plume involvement in the Emeishan flood-basalt province. *Geology* **2004**, *32*, 917–920. [[CrossRef](#)]
23. *Analysis Method for Clay Minerals and Ordinary Non-Clay Minerals in Sedimentary Rocks by the X-ray Diffraction*; SY/T 5163-2010; Petroleum Industrial Publishing House: Beijing, China, 2010. (In Chinese)
24. Brindley, G.W. Chemical compositions of berthierines—a review. *Clays Clay Miner.* **1982**, *30*, 153–155. [[CrossRef](#)]
25. Rivas-Sanchez, M.; Alva-Valdivia, L.; Arenas-Alatorre, J.; Urrutia-Fucugauchi, J.; Ruiz-Sandoval, M.; Ramos-Molina, M. Berthierine and chamosite hydrothermal: Genetic guides in the Pena Colorada magnetite-bearing ore deposit, Mexico. *Earth Planet. Space* **2006**, *58*, 1389–1400. [[CrossRef](#)]
26. Toth, T.A.; Fritz, S.J. An Fe-berthierine from a Cretaceous laterite: Part I. Characterization. *Clays Clay Miner.* **1997**, *45*, 564–579. [[CrossRef](#)]
27. Moore, D.; Hughes, R.E. Ordovician and Pennsylvanian berthierine-bearing flint clays. *Clays Clay Miner.* **2000**, *48*, 145–149. [[CrossRef](#)]
28. Moore, D.; Reynolds, R.C. *X-ray Diffraction and the Identification and Analysis of Clay Minerals*, 2nd ed.; Oxford University Press: Oxford, UK, 1997.
29. Zhao, L.; Graham, I. Origin of the alkali tonsteins from southwest china: Implications for alkaline magmatism associated with the waning stages of the emeishan large igneous province. *Aust. J. Earth Sci.* **2016**, *63*, 123–128. [[CrossRef](#)]
30. Spears, D.A. The origin of tonsteins, an overview, and links with seatearths, fireclays and fragmental clay rocks. *Int. J. Coal Geol.* **2012**, *94*, 22–31. [[CrossRef](#)]
31. Iijima, A.; Matsumoto, R. Berthierine and chamosite in coal measures of Japan. *Clays Clay Miner.* **1982**, *30*, 264–274. [[CrossRef](#)]
32. Dai, S.; Chou, C.-L. Occurrence and origin of minerals in a chamosite-bearing coal of Late Permian age, Zhaotong, Yunnan, China. *Am. Mineral.* **2007**, *92*, 1253–1261. [[CrossRef](#)]
33. Wang, X.; Dai, S.; Chou, C.-L.; Zhang, M.; Wang, J.; Song, X.; Wang, W.; Jiang, Y.; Zhou, Y.; Ren, D. Mineralogy and geochemistry of Late Permian coals from the Taoshuping Mine, Yunnan province, China: Evidences for the sources of minerals. *Int. J. Coal Geol.* **2012**, *96–97*, 49–59. [[CrossRef](#)]
34. Dai, S.; Li, T.; Seredin, V.V.; Ward, C.R.; Hower, J.C.; Zhou, Y.; Zhang, M.; Song, X.; Song, W.; Zhao, C. Origin of minerals and elements in the Late Permian coals, tonsteins, and host rocks of the Xinde Mine, Xuanwei, eastern Yunnan, China. *Int. J. Coal Geol.* **2014**, *121*, 53–78. [[CrossRef](#)]
35. Dai, S.; Tian, L.; Chou, C.-L.; Zhou, Y.; Zhang, M.; Zhao, L.; Wang, J.; Yang, Z.; Cao, H.; Ren, D. Mineralogical and compositional characteristics of Late Permian coals from an area of high lung cancer rate in Xuanwei, Yunnan, China: Occurrence and origin of quartz and chamosite. *Int. J. Coal Geol.* **2008**, *76*, 318–327. [[CrossRef](#)]
36. Dai, S.; Luo, Y.; Seredin, V.V.; Ward, C.R.; Hower, J.C.; Zhao, L.; Liu, S.; Zhao, C.; Tian, H.; Zou, J. Revisiting the Late Permian coal from the Huayingshan, Sichuan, southwestern China: Enrichment and occurrence modes of minerals and trace elements. *Int. J. Coal Geol.* **2014**, *122*, 110–128. [[CrossRef](#)]
37. Bohor, B.F.; Triplehorn, D.M. Tonsteins: Altered volcanic-ash layers in coal-bearing sequences. *Geol. Soc. Am. Spec. Pap.* **1993**, *285*, 1–44.

38. Deconinck, J.-F.; Crasquin, S.; Bruneau, L.; Pellenard, P.; Baudin, F.; Feng, Q. Diagenesis of clay minerals and K-bentonites in Late Permian/Early Triassic sediments of the Sichuan Basin (Chaotian section, central China). *J. Asian Earth Sci.* **2014**, *81*, 28–37. [[CrossRef](#)]
39. Ward, C.R. Analysis and significance of mineral matter in coal seams. *Int. J. Coal Geol.* **2002**, *50*, 135–168. [[CrossRef](#)]
40. Zhao, L.; Ward, C.R.; French, D.; Graham, I.T. Mineralogy of the volcanic-influenced Great Northern coal seam in the Sydney Basin, Australia. *Int. J. Coal Geol.* **2012**, *94*, 94–110. [[CrossRef](#)]
41. Ren, D. *Coal Petrology of China*; China University of Mining and Technology Press: Xuzhou, China, 1996. (In Chinese)
42. Wang, X.; Zhang, M.; Zhang, W.; Wang, J.; Zhou, Y.; Song, X.; Li, T.; Li, X.; Liu, H.; Zhao, L. Occurrence and origins of minerals in mixed-layer illite/smectite-rich coals of the Late Permian age from the Changxing Mine, eastern Yunnan, China. *Int. J. Coal Geol.* **2012**, *102*, 26–34. [[CrossRef](#)]
43. Spears, D.A.; Duff, P.M.D. Kaolinite and mixed-layer illite–smectite in lower cretaceous bentonites from the peace river coalfield, british columbia. *Can. J. Earth Sci.* **1984**, *21*, 465–476. [[CrossRef](#)]
44. Pevear, D.R.; Williams, V.E.; Mustoe, G.E. Kaolinite, smectite, and k-rectorite in bentonites: Relation to coal rank at tulameen, british columbia. *Clays Clay Miner.* **1980**, *28*, 241–254. [[CrossRef](#)]
45. Reinink-Smith, L.M. Mineral assemblages of volcanic and detrital partings in tertiary coal beds. *Clays Clay Miner.* **1990**, *38*, 97–108. [[CrossRef](#)]
46. Pellenard, P.; Deconinck, J.-F.; Huff, W.D.; Thierry, J.; Marchand, D.; Fortwengler, D.; Trouiller, A. Characterization and correlation of Upper Jurassic (Oxfordian) bentonite deposits in the Paris Basin and the Subalpine Basin, France. *Sedimentology* **2003**, *50*, 1035–1060. [[CrossRef](#)]
47. Deconinck, J.-F.; Amédéo, F.; Baudin, F.; Godet, A.; Pellenard, P.; Robaszynski, F.; Zimmerlin, I. Late cretaceous paleoenvironments expressed by the clay mineralogy of cenomanian-campanian chalks from the east of the paris basin. *Cretac. Res.* **2005**, *26*, 171–179. [[CrossRef](#)]
48. Vázquez, M.; Nieto, F.; Morata, D.; Droguett, B.; Carrillo-Rosua, F.J.; Morales, S. Evolution of clay mineral assemblages in the Tinguiririca geothermal field, Andean Cordillera of central Chile: An XRD and HRTEM-AEM study. *J. Volcanol. Geotherm. Res.* **2014**, *282*, 43–59. [[CrossRef](#)]
49. Somelar, P.; Kirsimäe, K.; Środoń, J. Mixed-layer illite-smectite in the Kinnekulle K-bentonite, northern Baltic Basin. *Clay Miner.* **2009**, *44*, 455–468. [[CrossRef](#)]
50. Hoffman, J.; Hower, J. Clay mineral assemblages as low grade metamorphic geothermometers: Application to the thrust faulted disturbed belt of Montana, USA. *SEPM Spec. Publ.* **1979**, *26*, 55–79.
51. Susilawati, R.; Ward, C.R. Metamorphism of mineral matter in coal from the Bukit Asam deposit, South Sumatra, Indonesia. *Int. J. Coal Geol.* **2006**, *68*, 171–195. [[CrossRef](#)]
52. Uysal, I.T.; Glikson, M.; Golding, S.D.; Audsley, F. The thermal history of the Bowen Basin, Queensland, Australia: Vitrinite reflectance and clay mineralogy of Late Permian coal measures. *Tectonophysics* **2000**, *323*, 105–129. [[CrossRef](#)]
53. Abid, I.A.; Hesse, R.; Harper, J.D. Variations in mixed-layer illite/smectite diagenesis in the rift and post-rift sediments of the Jeanne d’Arc Basin, Grand Banks offshore Newfoundland, Canada. *Can. J. Earth Sci.* **2004**, *41*, 401–429. [[CrossRef](#)]
54. Schegg, R.; Leu, W. Clay mineral diagenesis and thermal history of the Thonex Well, western Swiss Molasse Basin. *Clays Clay Miner.* **1996**, *44*, 693–705. [[CrossRef](#)]
55. Środoń, J.; Clauer, N.; Huff, W.; Dudek, T.; Banaś, M. K-Ar dating of the Lower Paleozoic K-bentonites from the Baltic Basin and the Baltic Shield: Implications for the role of temperature and time in the illitization of smectite. *Clay Miner.* **2009**, *44*, 361–387. [[CrossRef](#)]
56. Hornibrook, E.R.; Longstaffe, F.J. Berthierine from the Lower Cretaceous Clearwater Formation, Alberta, Canada. *Clays Clay Miner.* **1996**, *44*, 1–21. [[CrossRef](#)]
57. Jahren, J.S.; Aagaard, P. Compositional variations in diagenetic chlorites and illites, and relationships with formation-water chemistry. *Clay Miner.* **1989**, *24*, 157–170. [[CrossRef](#)]
58. Dai, S.; Graham, I.T.; Ward, C.R. A review of anomalous rare earth elements and yttrium in coal. *Int. J. Coal Geol.* **2016**, *159*, 82–95. [[CrossRef](#)]
59. Dai, S.; Wang, X.; Seredin, V.V.; Hower, J.C.; Ward, C.R.; O’Keefe, J.M.K.; Huang, W.; Li, T.; Li, X.; Liu, H.; *et al.* Petrology, mineralogy, and geochemistry of the Ge-rich coal from the Wulantuga Ge ore deposit, Inner Mongolia, China: New data and genetic implications. *Int. J. Coal Geol.* **2012**, *90–91*, 72–99. [[CrossRef](#)]

60. Środoń, J. Nature of mixed-layer clays and mechanisms of their formation and alteration. *Annu. Rev. Earth and Planet. Sci.* **1999**, *27*, 19–53. [[CrossRef](#)]
61. Hower, J.; Eslinger, E.V.; Hower, M.E.; Perry, E.A. Mechanism of burial metamorphism of argillaceous sediment: 1. Mineralogical and chemical evidence. *Geol. Soc. Am. Bull.* **1976**, *87*, 725–737. [[CrossRef](#)]
62. Peltonen, C.; Marcussen, Ø.; Bjørlykke, K.; Jahren, J. Clay mineral diagenesis and quartz cementation in mudstones: The effects of smectite to illite reaction on rock properties. *Mar. Pet. Geol.* **2009**, *26*, 887–898. [[CrossRef](#)]
63. Thyberg, B.; Jahren, J.; Winje, T.; Bjørlykke, K.; Faleide, J.I.; Marcussen, Ø. Quartz cementation in Late Cretaceous mudstones, northern North Sea: Changes in rock properties due to dissolution of smectite and precipitation of micro-quartz crystals. *Mar. Pet. Geol.* **2010**, *27*, 1752–1764. [[CrossRef](#)]



© 2016 by the authors; licensee MDPI, Basel, Switzerland. This article is an open access article distributed under the terms and conditions of the Creative Commons Attribution (CC-BY) license (<http://creativecommons.org/licenses/by/4.0/>).